Cryogenic DT and D_2 Targets for Inertial Confinement Fusion

Introduction

Laboratory-based ignition via inertial confinement fusion (ICF)[1] will be achieved by imploding a spherical capsule containing a frozen layer of deuterium and tritium (DT) fuel on the MJ-class National Ignition Facility (NIF)[2] currently under construction at Lawrence Livermore National Laboratory (see Fig. 108.1). Virtually all ICF ignition target designs are based on a spherical low-Z ablator containing a solid, cryogenic DT-fuel shell surrounding a low-density DT vapor at, or slightly below, the triple point. There are two fundamental target designs for ignition: capsules directly illuminated by the laser (direct drive[3]) and capsules driven by a uniform x-ray radiation field created by illuminating the inside surface of a high-Z cylindrical hohlraum (indirect drive[4]). Figure 108.2 illustrates the drive concept and capsule design for both direct- and x-ray-drive ignition targets. X-ray-drive ignition capsules[5] are based on a thick, copper-doped Be ablator surrounding a relatively thin DT-ice layer; capsules for direct-drive ignition[3] consist of a very thin plastic shell surrounding a relatively thick DT-ice layer. When these capsules are illuminated by either the laser or the x-ray field inside a hohlraum, the ablator material is rapidly heated and driven away from the capsule. The resulting shock compresses the DT-fuel shell, raising the pressure in the central gas region (or core) to several Mbar. Once the laser irradiation ceases, the fuel shell begins to decelerate, further compressing and heating the core as the shell's kinetic energy is converted to thermal energy via PdV work. To initiate a thermonuclear burn, the temperature and areal density of the core must reach approximately 10 keV and 300 to 400 mg/cm^2, respectively.[4] Under these conditions, the rate of energy deposited in the fuel by the 3.5-MeV ^{4}He nuclei from the DT–fusion reaction is greater than the energy lost by electron conduction or x-ray emission, and a thermonuclear burn wave propagates through the dense fuel shell in a few tens of picoseconds. This is much shorter that the fuel-disassembly time of a few hundred picoseconds.

1.8 MJ

Under construction at LLNL
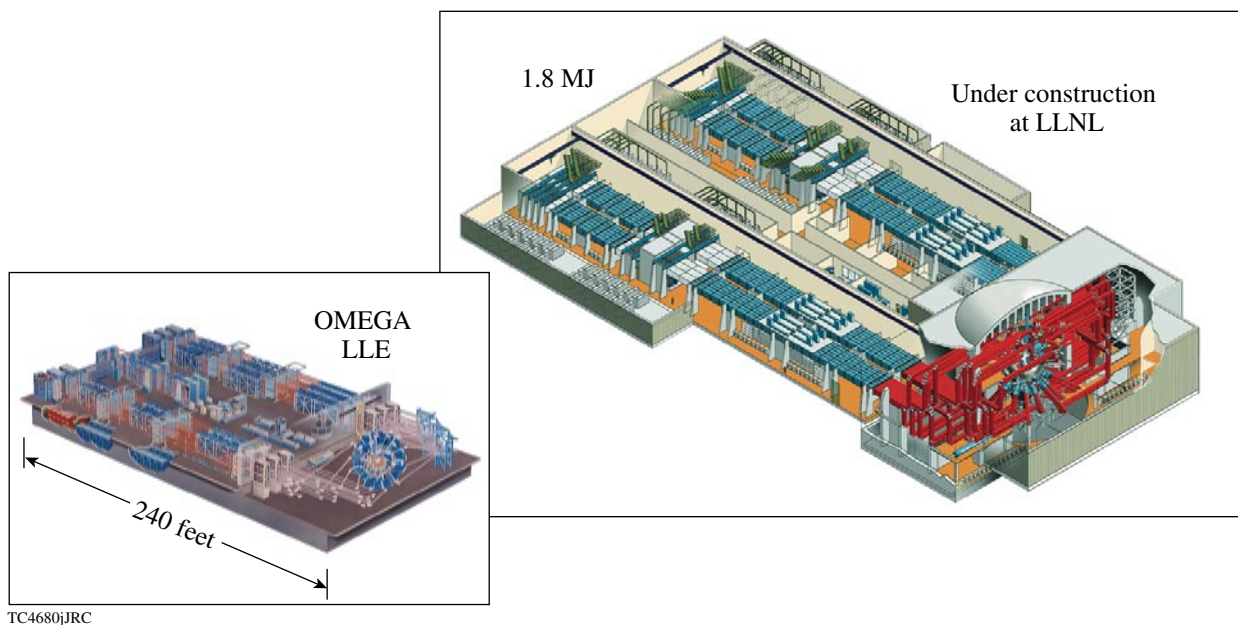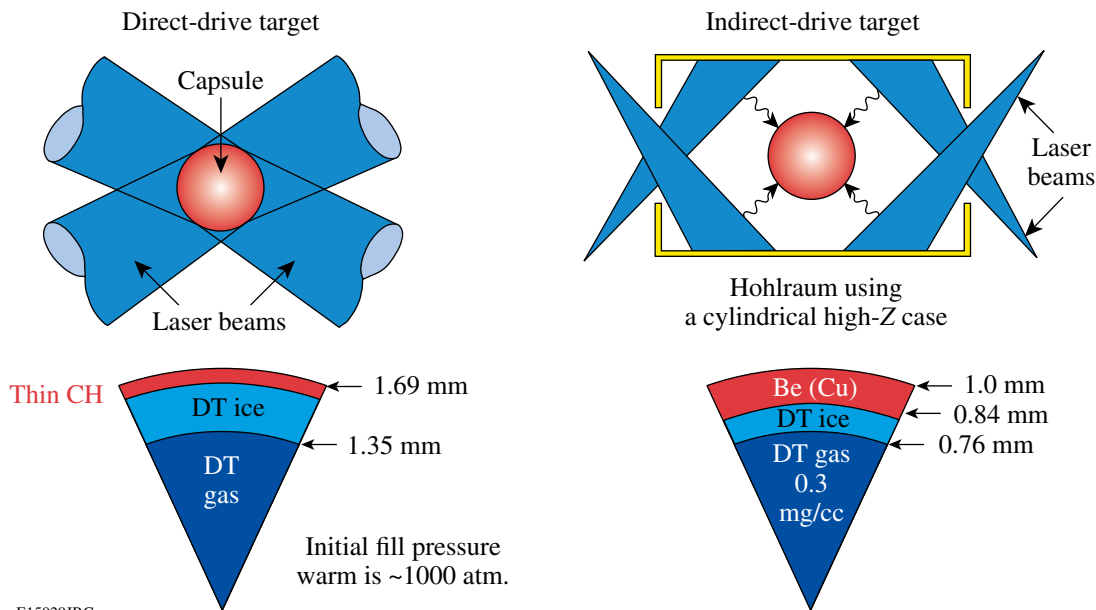
OMEGA LLE

240 feet

TC4680jRC

Figure 108.1
The National Ignition Facility (NIF) is under construction at Lawrence Livermore National Laboratory and will begin ignition experiments with cryogenic DT targets in 2010. LLE's OMEGA laser is being used to develop the scientific and technical basis for ignition on the NIF. OMEGA performs 40 to 50 cryogenic D_2 and DT implosions annually in support of the ignition mission.

Direct-drive target

Capsule

Laser beams

Thin CH

DT ice

1.69 mm

1.35 mm

DT gas

Initial fill pressure
warm is ~1000 atm.

E15029JRC

Indirect-drive target

Laser
beams

Hohlraum using
a cylindrical high-Z case

Be (Cu)

DT ice

DT gas
0.3
mg/cc

1.0 mm

0.84 mm

0.76 mm

Figure 108.2
The basic ignition-target designs are shown along with the fundamental concepts for direct and indirect (or x-ray) drive.

For nearly two decades, LLE has been developing the scientific and engineering basis to create and characterize cryogenic DT capsules and to study the implosion performance under scaled-ignition conditions. Cryogenic fuel shells are the preferred configuration for ICF because the fuel can be compressed isentropically, minimizing the laser energy required to achieve ignition conditions.[6] Since beginning cryogenic target implosions on the 60-beam, 30-kJ UV OMEGA laser[7] (see Fig. 108.1), 118 cryogenic D_2 (Refs. 8–11) and 15 cryogenic DT capsules have been imploded. While the compressed-fuel densities and core temperatures of these cryogenic DT implosions will never meet the criteria for ignition, measured fuel areal densities (the product of the fuel density and the radial extent of the fuel) have been inferred in excess of 100 mg/cm^2. This is an important step toward the demonstration of energy gain via ICF and ultimately the realization of inertial fusion energy.[12]

The uniformity of the inner surface of the DT-ice layer is one of the critical factors that determine target performance.[3,4] As the high-density fuel shell decelerates and compresses, inner-surface perturbations grow due to the Rayleigh–Taylor instability.[13] These perturbations include ablation-front features that feed through the fuel shell[14] and native inner-ice-surface roughness from the layering process described in **Cryogenic D_2 and DT Target Fabrication and Characterization** (p. 170). The ablation-front perturbations are generated primarily by laser non-uniformities and the feedout of inner-ice-surface perturbations carried by the reflected shock. These ablation-front perturbations can be controlled by conditioning the laser pulse[15] or by careful design of the hohlraum used to create a homogenous radiation field around the capsule for indirect drive.[16] If the initial amplitude of the inner-surface perturbations is too large, the hot core is disrupted and the conditions for ignition and burn do not occur. This leads to an ignition requirement that the inner-surface ice roughness be less than 1-μm rms in all modes.[3,4]

The OMEGA laser is the only facility in the world routinely imploding cryogenic D_2 and DT targets. The target-handling concepts on OMEGA are based on work that began nearly 30 years ago. The next section will review some of the historical accomplishments that had a direct impact on the design of the OMEGA system. One of the fundamental breakthroughs for ignition was the realization of β-layering in 1986. The next section will also describe the β-layering process. Later sections will (1) discuss the development of optical and x-ray-characterization techniques to assess the quality of the DT layers produced by β-layering; (2) describe the systems used to implode these targets on the OMEGA and NIF lasers; and (3) present the results of the first cryogenic DT implosions on OMEGA.

Historical Perspective

Following the concept declassification, J. H. Nuckolls *et al.* first discussed the concept of laser fusion in 1972.[1] Powerful lasers would be used to implode a shell or sphere of solid DT reaching breakeven at relatively modest laser energies (at least by today's standards). While the physical assumptions in this

and other early work turned out to be overly optimistic with respect to the required laser energy, the basic target design—a shell of solid DT—has remained unchanged. After this seminal publication appeared, work began on the development of target concepts for creating thin cryogenic-DT layers (both solid and liquid). The early work (throughout much of the 1970s and 1980s) focused on thin glass shells filled with high-pressure DT gas. Typical scales were 100-μm-diam shells with up to 100 atm of DT gas. When cooled using thermal conduction, the DT layers were typically less than 10 μm thick.

In 1977, Henderson and Johnson at KMS Fusion[17] reported the first irradiation of a cryogenic DT capsule with a laser. The target was a 60-μm-diam, thin-walled glass shell filled with 10 atm of DT (60:40). The capsule was cooled via point-contact conduction and was exposed to ambient chamber infrared (IR) radiation (the point-contact cooling overwhelmed the IR heating from the chamber). These capsules were illuminated with a laser power of approximately 0.2 TW and produced a neutron yield between 10^6 and 10^7, an order of magnitude higher than the same capsules illuminated at room temperature. This demonstrated the advantage of using the high-density cryogenic-fuel layer for ICF. At about the same time, Miller[18] described a new method for producing cryogenic-fuel layers based on what came to be known as the fast-refreeze technique. This technique produced layers with a considerably more uniform thickness than point conduction. The fast-refreeze technique relies on a static heat-exchange gas (He) for rapid cooling of the capsule. Once frozen, the ice in the capsule is melted using a laser beam. The vapor then condenses uniformly on the inside of the glass shell and refreezes before gravity can induce the liquid to flow. This technique quickly became the standard for cryogenic target development well into the 1980s.

In 1978, Musinski *et al.*[19] adapted the fast-refreeze technique for the targets being imploded at KMS Fusion. To eliminate the He exchange gas prior to laser illumination and to minimize the exposure of the cold capsule to ambient IR radiation in the target chamber, they introduced the principle of a cryogenic retractable shroud. Here, the exchange gas is limited to a small volume around the capsule inside the shroud. Their calculations suggested that the exposure time had to be less than 10 ms once the shroud was removed or the thin DT-ice layer would melt due to ambient chamber IR radiation. Thus, within only a few years, three of the key concepts underpinning the success of the OMEGA Cryogenic Target Handling System had been developed: (1) redistribution of the ice using external radiation, (2) thermal control of the capsule isotherm via a cold exchange gas, and (3) a fast retractable shroud to minimize the target exposure to ambient chamber radiation. These concepts were employed on the 24-beam OMEGA laser[20] in 1987 and 1988 to implode over 100 cryogenic-DT-filled, fast-refreeze glass capsules leading to compressed DT densities of 100 to 200 times liquid density.[21]

By the late 1980s, it was realized that the fast-refreeze technique could not be used to create thick, uniform DT-fuel layers. Thicker DT layers were required for the advanced targets being designed for the proposed upgrade of the OMEGA laser to 60 beams and 30-kJ UV. Fundamentally, the thin glass shell exploding pusher targets originally envisioned for ignition and gain did not work. The demonstration of β-layering in 1988 by Hoffer and Foreman[22] revolutionized the development of targets for ICF and fusion ignition. The "β-heating" concept to produce highly uniform DT-ice layers inside capsules had been suggested by Martin as early as 1985 (Ref. 23) and published formally in 1988 (Ref. 24). The concept is deceptively simple. The radioactive decay of the tritium produces an electron with an average energy of about 6 keV. At 6 keV, the electron range in solid DT is only 1 to 2 μm, so the energy is deposited locally and, consequently, the bulk of the ice is heated uniformly. With a spherically symmetric isotherm on the capsule surface, the radial temperature gradient induced by the β-heating causes DT to sublimate from the slightly thicker and, consequently, slightly warmer regions inside the capsule and deposit on the slightly cooler, thinner regions (see Fig. 108.3). If the capsule surface is kept just below the triple point, the ice will ultimately relax to a uniform radial thickness.
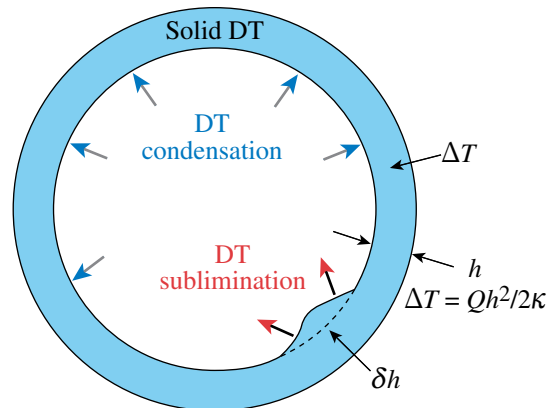

E15072JRC

Figure 108.3
Schematic showing the basic concept behind β-layering in a cryogenic DT shell. If the outside of the shell is maintained at a temperature slightly below the DT triple point, a temperature gradient develops across the ice due to the radioactive decay of the tritium; the emitted electron (average energy of 6 keV) deposits energy, locally heating the bulk of the ice. Consequently, radially thicker (warmer) regions sublimate inside the shell and condense on radially thinner (cooler) locations, eventually relaxing to a uniformly thick shell.

In 1996, Collins *et al.*[25] showed that IR radiation could be used to excite the vibration–rotation band in solid D_2 (or HD), leading to a redistribution or smoothing similar to that induced by β-layering in DT. The process is virtually identical to β-layering as the IR heats the bulk of the ice. With symmetric IR illumination and adequate power, the layer uniformity in D_2 should be as good as in DT.[26] In this way, cryogenic D_2 capsules can be used as ignition surrogates without the radiological impacts associated with DT (e.g., tritium contamination, neutron activation, neutron-induced radiation effects in diagnostics, etc.). Indeed, as mentioned in the **Introduction** (p. 167), the initial ignition-scaled cryogenic capsule implosions on OMEGA were based on D_2 fuel; DT was introduced only recently following extensive operational experience and a thorough systems readiness review.

Cryogenic D_2 and DT Target Fabrication and Characterization

Physically mounting a capsule to be imploded by a multi-beam laser system presents a great challenge for both direct- and x-ray-drive illumination. Mounting the capsule can have a profound effect on the resulting layer quality due to the thermal perturbations caused by the structures around the capsule. Target performance requires a high degree of irradiation uniformity (i.e., the capsule surface cannot be shadowed) and minimal mass perturbations on the surface of the capsule (some mechanical structure must physically attach to the capsule).

To meet these criteria for a direct-drive capsule, LLE implemented a concept based on spider silks[27] [see Fig. 108.4(a)]. Here the capsule is mounted at the center of a "C"-style frame using four strands of spider silk (the silk diameter is typically less than 1 μm). The strands are either glued directly to the surface of the capsule or the entire assembly is overcoated with a thin layer (typically 0.2 μm) of parylene to bond the silks to the capsule. The diameter of the cryogenic targets imploded on the OMEGA laser is set by scaling the ignition target design for the NIF to the energy available;[3] this leads to a capsule diameter of 860 μm for implosions on the OMEGA laser.

For OMEGA, these thin CH shells are permeation filled with an equimolar mixture of DT to 1000 atm. At pressure, the shell and gas are slowly cooled to a few degrees below the DT triple point (19.8 K), while the pressure differential across the shell is maintained below 1 atm to avoid buckling. This is the most critical step in the filling process. Once the DT gas solidifies, the capsule is transferred to a moving cryostat;[8,9] this cryostat is used to maintain the appropriate thermal environment around the capsule until it is imploded. Inside the moving cryostat, the capsule is kept at the center of a gold-coated copper layering
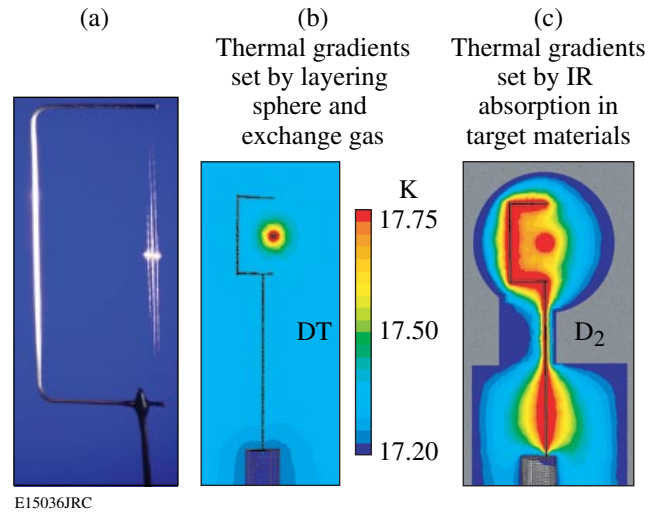

(a)   (b) Thermal gradients set by layering sphere and exchange gas   (c) Thermal gradients set by IR absorption in target materials

K
17.75
17.50
DT
17.20

D₂

E15036JRC

Figure 108.4

(a) To create a cryogenic target, an 860-μm-diam CH shell is initially mounted to a beryllium "C"-style frame using four strands of spider silk. (b) Thermal modeling shows that isotherm at the surface of a cryogenic DT-filled capsule is highly uniform. (c) However, the IR radiation used to layer D_2 ice also heats the beryllium "C"-mount and the spider silks, causing a significant distortion in the isotherm at the surface of the capsule. This can lead to a significant asymmetry in the ice thickness for cryogenic D_2 targets.

sphere with two orthogonal viewing ports for alignment and ice-surface characterization (discussed below). A thermal model of this system [see Figs. 108.4(b) and 108.4(c)] shows that the isotherm at the surface of a DT capsule is spherical and that none of the target-support structures or layering-sphere asymmetries (e.g., sapphire windows for viewing the target) influence the isotherm [Fig. 108.4(b)]. By controlling the pressure of the exchange gas and the temperature of the copper layering sphere, a spherical isotherm at the DT triple point can be maintained at the ice surface inside the capsule and β-layering produces high-quality layers within a matter of hours.

With IR illumination, the thermal model indicates that there can be significant geometrical distortions in the capsule surface isotherm [Fig. 108.4(c)]. These distortions are caused by IR radiation absorbed on the target support structures (the Be C-mount and the silk).[26] For example, the D_2 ice facing the Be C-mount is typically thinner since the Be frame is warmer than the He exchange gas. This modeling suggested three changes that significantly improved the D_2-ice-layer quality: (1) the pressure of the exchange gas was increased to further homogenize the thermal perturbations, (2) the target structures were plated with gold to reduce the IR absorption, and (3) a diffuser was added to the IR heating port to more uniformly distribute the radiation in the layering sphere (which acts as an integrating sphere for
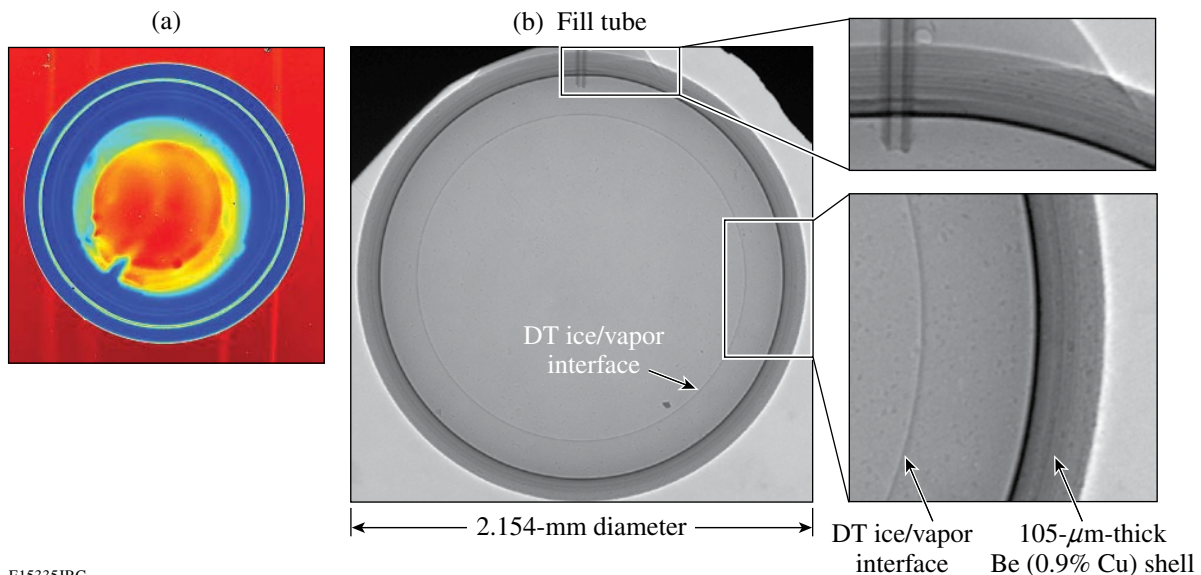
the IR). With these improvements, the average ice-layer quality in D_2 capsules improved by a factor of 2.

For x-ray drive on the NIF, Be capsules are mounted at the center of a cylindrical high-Z hohlraum using a "tenting" scheme.[5] The thermal environment around the capsule is established by the hohlraum geometry. Azimuthally symmetric heaters are placed along the hohlraum axis to produce a more spherically symmetric isotherm at the capsule surface.[28] The Be shells are filled in generally less than 30 min using a narrow fill tube connected to a DT reservoir. Simulations suggest that the fill-tube perturbation will not significantly affect implosion performance.[29] The β-layering process inside the hohlraum has been rigorously tested in the laboratory and will be incorporated into the Load, Layer, and Characterization System (LLCS) under development for the NIF Cryogenic Target System (NCTS). Once a uniform layer is achieved, the temperature of the ice is cooled further to reduce the DT vapor density in the central void region. At 1.5 K below the triple point, the vapor density is 0.3 mg/cc; this is the x-ray-drive-ignition requirement. Cooling the capsule below the triple point is not a requirement for the baseline direct-drive-ignition design.

Apart from the need to monitor the ice layers during formation, simulation codes require inner-ice-surface characterization information to properly predict target performance; therefore, it is important to image the liquid/ice-layer surface with high resolution. For transparent ablators (e.g., CH or CD shells), the location of the inner ice surface is measured using optical shadowgraphy.[30] The capsule is backlit using an optical plane wave (typically a pulsed source with a duration of less than 1 ms to minimize any motional blurring; the energy absorbed by the capsule is negligible). The light is totally internally reflected off the inner surface of the ice, creating a bright ring in the image plane that represents the location of the inner surface relative to the center of the capsule. This bright ring can be seen in Fig. 108.5(a)—a shadowgraph of the first DT capsule to achieve an inner-ice-surface smoothness of 1-μm rms. The resolution of the shadowgraph is less than 0.1 μm. The ring represents an azimuthal measure of the radial variation of the ice along a slice through the center of the capsule normal to the optical viewing axis. This ring is "unwrapped" azimuthally around the center of the capsule to form a line in radius-azimuth space. A power spectrum of the ice roughness as a function of the mode number is generated by fitting the Fourier amplitudes of the radial variation as a function of the azimuth.[31]

For opaque ablators (e.g., Be or low-density foams), x-ray phase-contrast imaging is used to determine the location of the inner ice surface.[32] Phase-contrast imaging relies on spatial gradients in the real part of the refractive index to produce image contrast. These gradients occur at the Be/ice and ice/vapor (the

(a)   (b) Fill tube

DT ice/vapor interface

|← 2.154-mm diameter →| DT ice/vapor interface   105-μm-thick Be (0.9% Cu) shell

E15335JRC

Figure 108.5
(a) A typical optical shadowgraph of a cryogenic DT layer. The bright band is a measure of the radial variation of the inner ice surface for a slice through the center of the target. (b) A typical x-ray phase-contrast image of a beryllium shell containing a DT-ice layer. The phase-contrast image provides structural detail within the shell and the ice. The inner band represents a measure of the radial variation of the inner ice surface along a slice through the center of the capsule.

central void region) interfaces of a layered target, causing local curvature in the transmitted wave that leads to interference and a modulation in the x-ray intensity. Even for a virtually transparent medium (e.g., the region around the interface of the ice and DT vapor), phase gradients modulate the intensity of an x-ray wave and can be used to determine the precise location of the ice surface along a slice through the capsule normal to the x-ray-propagation axis. Figure 108.5(b) shows an example of an x-ray phase-contrast image. The capsule is a 105-μm-thick Be shell containing an ~180-μm-thick DT-ice layer. The ice/vapor interface is unwrapped in radius-azimuth space, and a power spectrum as a function of the mode number is generated as described above.

Because of the inherent symmetry of the direct-drive layering sphere, it is possible to rotate a direct-drive capsule with respect to the viewing axes in the characterization station. By rotating the capsule, any number of independent shadowgraphs can be obtained and used to create a 3-D representation of the inner ice surface. Such a representation (based on 48 independent shadowgraphs) is shown in Fig. 108.6 for two different DT-ice layers. Since the viewing axes are not orthogonal to the rotation axis, the poles of the capsules cannot be characterized. The contours represent surface deviations in microns relative to a perfect sphere at the average ice-surface radius. The peak-to-valley surface variation for both capsules is ~2 μm out of a total ice thickness of ~95 μm. Full $Y_{\ell m}$ Legendre amplitudes can be fit to this surface for modes up to 12 (the limiting factor is the missing data at the poles), and the procedure described by Hatchett and Pollaine[33] is used to estimate the 2-D equivalent of the Legendre modes for $\ell > 12$. The ignition specification is typically quoted as a power spectrum for modes from 1 to 1000, although in practice the resolution of the measurement limits meaningful power to modes less than 100 or so.[34] For direct drive, this specification is 1.0-μm rms in all modes and $\leq$0.25-μm rms in modes greater than 10. Both of the targets shown in Fig. 108.6 meet the inner-ice-surface smoothness requirement for direct-drive ignition on the NIF. Figure 108.7 compares the power-spectrum decomposition of the ice-surface roughness for six targets imploded consecutively on the OMEGA laser and the ignition specification (heavy solid line). For the best capsule, the measured power spectrum is 0.72-μm rms in all modes and 0.24-μm rms above mode 10, comfortably exceeding the ignition requirement.

Layering and characterization of a DT-fuel layer in a hohlraum for x-ray-drive ignition present significant challenges. For capsules in a hohlraum, the presence of the fill tube can create a thermal asymmetry leading to a low-mode variation in the ice thickness around the fill tube (generally thicker ice since the fill
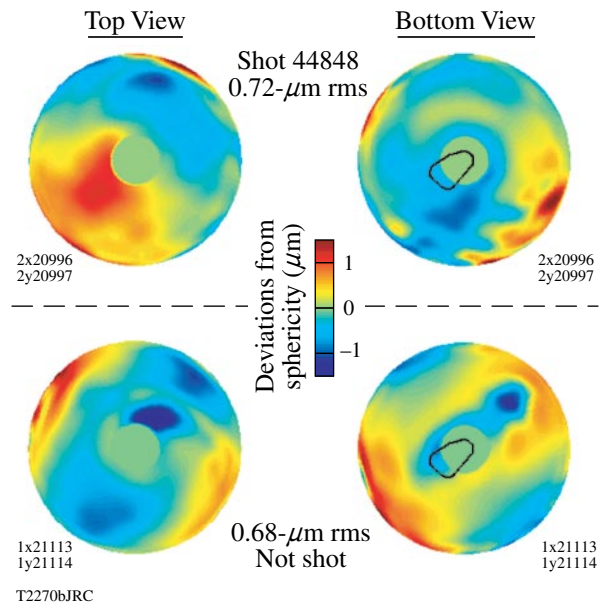

Figure 108.6
A 3-D representation of the inner ice surface can be created by fitting to a large number of independent shadowgraphs. Top and bottom views are shown for two different capsules that meet the direct-drive-ignition requirement for the inner ice smoothness. The contour mapping represents deviations of the inner ice surface from a sphere at the average radius. Because the viewing axes are not orthogonal to the rotation axis, there is no data at the poles.
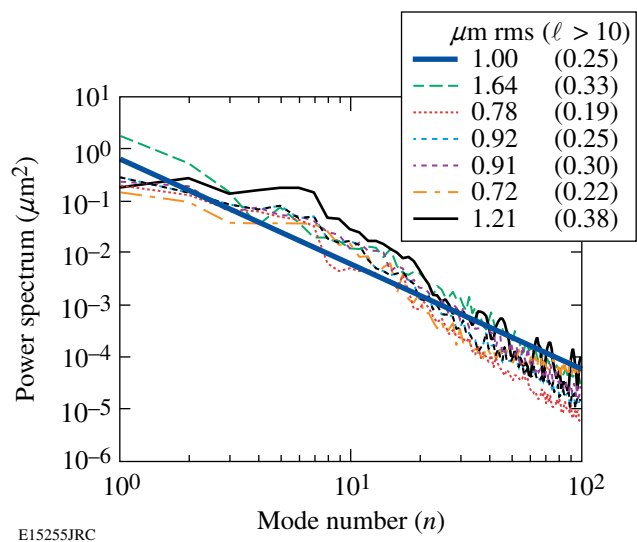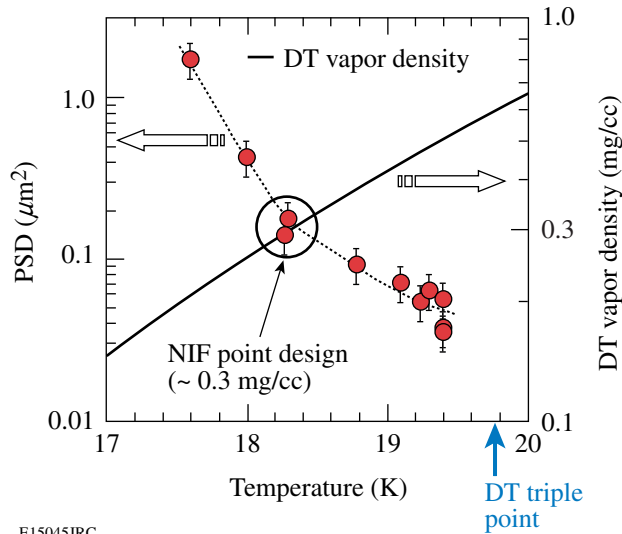

Figure 108.7
The power per mode for six DT cryogenic targets as a function of mode number. These targets were shot consecutively over a period of several weeks on OMEGA. The direct-drive-ignition specification for the inner ice smoothness is shown as the heavy solid line.

tube is colder). Furthermore, as the ice as cooled below the triple point, mid- and high-mode roughness begins to appear as the ice contracts and the β-layering process begins to shut down. However, by cooling very slowly from the triple point to 18.3 K (the ignition requirement), the ice roughness remains at the ignition specification for modes 10 and above. The behavior of the ice roughness in modes 10 to 128 as a function of ice temperature is shown in Fig. 108.8.
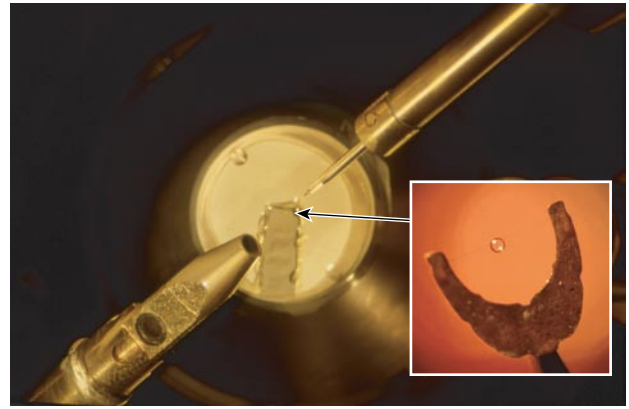

Figure 108.8

The power-spectral density for a prototype x-ray-drive cryogenic DT target as a function of the ice temperature. The power spectral distribution (PSD) is summed for modes 10 to 128. The ice-temperature requirement for x-ray-drive ignition is 18.3 K. This target meets the ignition requirement over this mode range at the required ice temperature.

Imploding Cryogenic Targets on OMEGA and the NIF

The original Cryogenic Target Handling System (CTHS) on the 24-beam OMEGA laser[20] incorporated the concepts discussed in **Historical Perspective** (p. 168). These concepts included an opposed-port shroud-retraction scheme using a linear induction motor and He gas cooling to support the fast-refreeze layering process. A shearing interferometer was implemented for layer characterization (thickness and uniformity). The thermally passive shroud and the actively cooled target stalk are shown in Fig. 108.9. The inset picture in Fig. 108.9 shows the "horseshoe" target assembly with a 300-μm-diam glass shell mounted using several strands of spider silk (rather than using glue to bond the silk to the capsule, the capsule and silk were overcoated with 0.2 μm of parylene following assembly). During the late 1980s, this system imploded over 100 glass-shell targets with 5-μm-thick DT layers, achieving 200 times liquid density in the DT.[21]

Figure 108.9

The shroud and target inserter from the 24-beam OMEGA Cryogenic Target Handling System are shown. The thermally passive removable shroud is the structure at the lower left. The inset shows a picture of the "horseshoe"-style mount for the capsule. Strands of spider silk are used to mount the capsule between the tips of the mount.

By the early 1990s, target designs were being developed for ignition that required considerably thicker DT layers with very high layer uniformity.[35] The fast-refreeze technique and thin glass shells were no longer adequate. New concepts were developed by General Atomics and LLE to support scaled-ignition target implosions on the new 60-beam OMEGA laser (completed in 1996). The new requirements for the CTHS included (1) a separate high-pressure-permeation fuel-filling system that was both D$_2$ and DT capable, (2) variable ice-layer thickness up to 100 μm in mm-diameter-scale, thin-walled CH capsules, (3) the capability to fill up to 12 targets per week, (4) IR-enhanced layering for D$_2$ and β-layering for DT fuel, (5) an independent layer-characterization station based on optical shadowgraphy, (6) a moving cryostat to deliver the target from the tritium facility to the target chamber, (7) target-alignment accuracy relative to the target chamber center (TCC) of 5 μm, (8) an opposed-port shroud-retraction scheme with a target exposure time of less than 100 ms before laser irradiation, and (9) a vertical shroud pull.

The operation of the CTHS on OMEGA has been well documented.[8–11] Since 2001, 118 cryogenic D$_2$ and 15 cryogenic DT capsules have been imploded. The key to the success of the OMEGA CTHS is the moving-cryostat concept. A photograph of the moving cryostat is shown in Fig. 108.10 with and without the thermally passive upper shroud. The moving cryostat includes a local He-gas cryogenic cooler on the thermally controlled lower shroud, a four-axis position controller (X, Y, Z, and θ) for the target stalk, a rigid docking interface to the target chamber, He exchange-gas regulation, and a thermally passive upper shroud with sapphire windows aligned to the OMEGA Target

Viewing System. With the moving-cryostat concept, critical target functions are performed away from the target chamber (i.e., permeation filling, layering, and characterization). Consequently, there is little or no impact on the utilization of the laser system when imploding cryogenic targets. An overview of the target handling process is shown in Fig. 108.11. The targets are permeation filled in a separate cryostat over a period of approximately four days and then transferred to the moving cryostat. The moving cryostat is then mated to the Characterization Station (still within the tritium facility). Once the appropriate layer is achieved (this typically requires 1 to 2 days for D_2 and less than 1 day for DT), the moving cryostat is taken to the bay beneath the OMEGA target chamber (a distance of about 200 ft). The moving cryostat is aligned with the lower pylon and then raised 22 ft through a vacuum interface to the center of the target chamber. Target alignment is performed using an automated centering routine to predetermined coordinates that account for static alignment offsets due to the sapphire windows. At shot time, a linear induction motor (LIM) removes the upper shroud using a precise acceleration/deceleration trajectory. The trajectory minimizes mechanical coupling between the LIM motion and the target. The target is exposed to the ambient chamber radiation for 90 ms prior to laser irradiation.

The conceptual basis for the NIF Cryogenic Target System (NCTS)[28,36] is significantly different from the OMEGA CTHS. The Load, Layer, and Characterization System (LLCS) is being developed to operate just outside the NIF target chamber but mechanically integrated with the target inserter and target chamber. Using the LLCS, DT will be loaded at about 50 psi into a 1-cc reservoir at the target base. This reservoir is connected to the Be capsule via a narrow (of the order of 10-μm OD) fill tube. The entire assembly is cooled to within a few degrees of the DT triple point (19.8 K). The reservoir is then heated to between 50 and 70 K, causing the DT to condense inside the Be shell. X-ray phase-contrast imaging will be used to monitor the DT meniscus (and consequently the amount of fuel in the shell) during the fill. Once the required amount of fuel is in the shell, the layering and characterization process proceeds as described in **Cryogenic D_2 and DT Target Fabrication and Characterization** (p. 170). Following the final characterization, the target is moved to the center of the NIF target chamber and aligned with the 192 laser beams. The target is protected from condensation and room-temperature IR radiation from the chamber by a clam-shell shroud (see Fig. 108.12). Several seconds before the shot, the shroud is opened. Heaters on the hohlraum compensate for the sudden IR illumination and maintain a constant hohlraum temperature. Any target vibration induced by the shroud opening damps during the 1 to 2 s prior to laser illumination.

Cryogenic DT Target Performance

All of the DT (and a few of the recent D_2) capsules imploded to date on OMEGA have been driven with a laser pulse designed to keep the fuel on an adiabat α of approximately 1 to 3, where α is the ratio of the internal pressure to the Fermi-degenerate pressure.[3]

With upper shroud removed

With upper shroud in place

Target assembly

Moving cryostat stalk

Upper shroud

Docking interface to lower pylon

Lower shroud

Four-axis target positioner
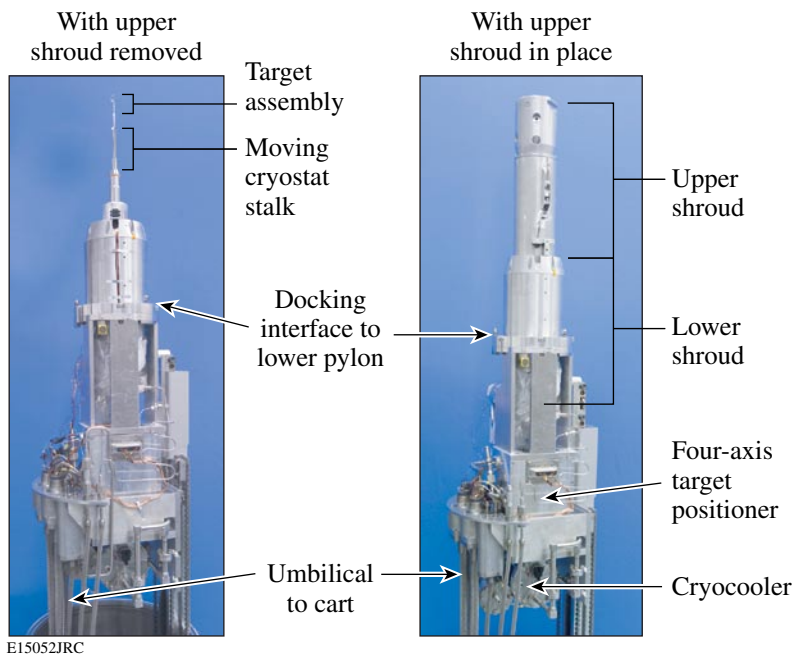
Umbilical to cart

Cryocooler

E15052JRC

Figure 108.10
The 60-beam OMEGA moving cryostat with (right) and without (left) the upper shroud. The moving cryostat is the heart of the OMEGA Cryogenic Target Handling System. The upper shroud is removed to expose the capsule at shot time. The capsule exposure time is approximately 90 ms.
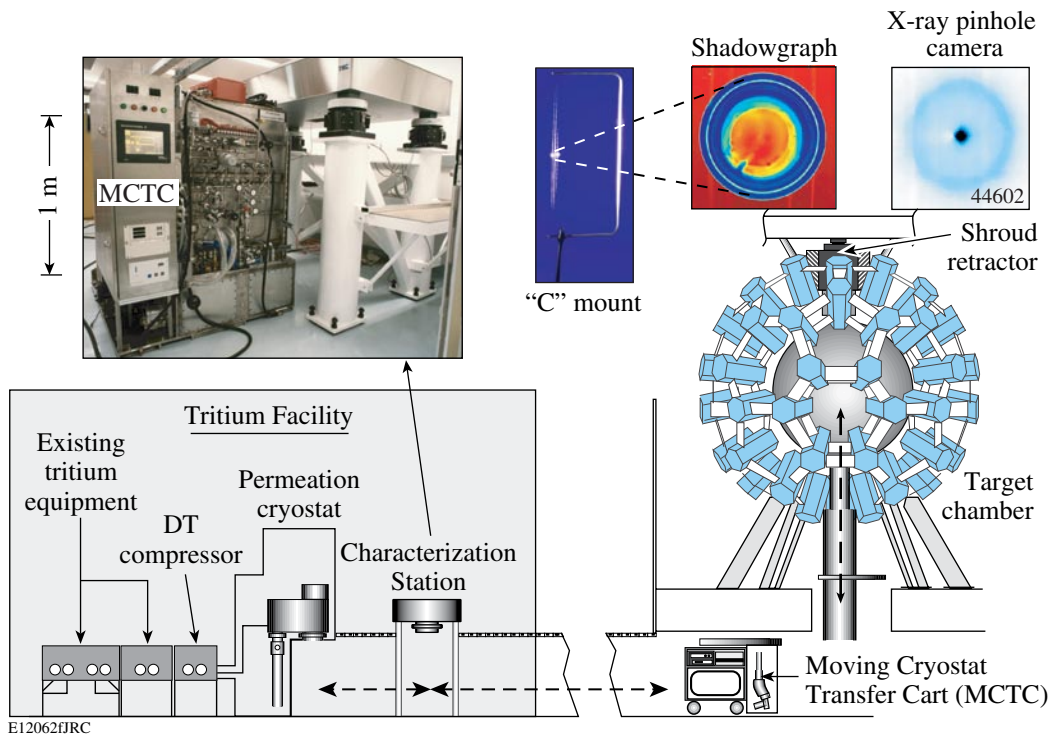
Figure 108.11

Target-handling operations are conducted away from the target chamber to increase the utilization of the laser facility. This includes the filling, layering, and characterization steps that are done within the LLE tritium facility. Once a target is ready to implode, the Moving Cryostat Transfer Cart (MCTC) is positioned below the chamber and the moving cryostat with the target is raised 22 ft to dock with the support structures on the target chamber. The entire shot sequence can be repeated approximately every 2 h.
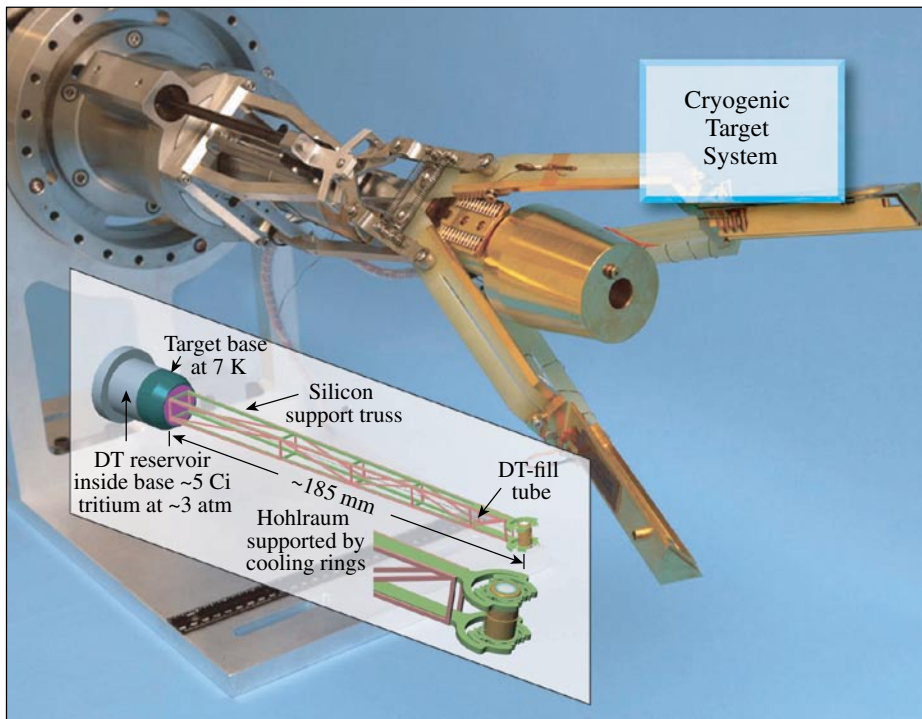

Figure 108.12

An x-ray-drive target on the NIF will be protected from the ambient chamber radiation using a clam-shell-style retractor. The clam-shell retractor can be opened slowly to avoid inducing excessive vibration because the target can withstand several seconds of chamber exposure before significant temperature perturbations develop on the capsule surface. The hohlraum/reservoir schematic shown in the inset fits on the end of the cold head in the middle of the figure.

These drive pulses scale to ignition, and consequently the areal densities during the fusion burn are expected (based on a 1-D radiation hydrocode simulation[36]) to be in excess of 200 mg/cm² (this corresponds to ~300× liquid density for the DT) and to approach 250 mg/cm² at peak density. The areal density monotonically increases during the fusion burn, and the neutron- or burn-averaged areal density $\langle \rho R \rangle_n$ will be less than the peak areal density ρR_{peak}. The fusion burn truncates prior to peak density (or compression) due to the thermal quenching caused by mixing of colder fuel with the hot spot.[37] Charged-particle diagnostics[38] are used to infer $\langle \rho R \rangle_n$ from D_2 implosions, while x-ray diagnostics[39] are used to infer ρR_{peak} from both D_2 and DT implosions.

The energy loss of secondary protons in the compressed D_2-fuel shell shows that the neutron-averaged areal density for $\alpha \sim 2$ implosions is as high as 100 to 110 mg/cm². A secondary proton spectrum from shot 45009 is shown in Fig. 108.13. The figure shows both the measured spectrum (solid circles with statistical error bars) and the birth spectrum (shaded region) in the core. The average energy loss in the dense-fuel shell is several MeV, corresponding to an areal density of 110 mg/cm². The low-energy tail suggests considerable low-mode instability growth late in time. These late-time protons probe regions of significantly higher fuel areal density but not necessarily regions representative of the overall shell areal density. For example, the
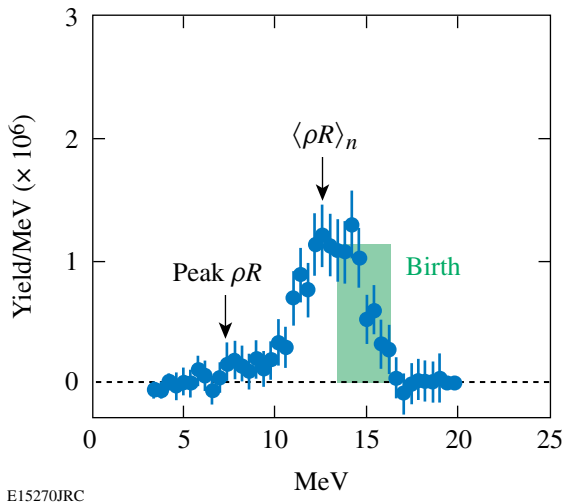
end point of this spectrum (at about 7 MeV) would correspond to an areal density of approximately 250 mg/cm² (based on a total dE/dx of over 5 MeV). For higher-yielding implosions, the areal-density evolution during the burn $\rho R(t)$ can be fit based on the technique described by Frenje and Smalyuk.[40]

The ρR_{peak} can be inferred based on the opacity of the shell by using the core self-emission to effectively backlight the shell. Figure 108.14 shows the measured x-ray spectrum from the core of shot 44948. This shot used a drive pulse to put the fuel shell on an adiabat close to 1. Since the x rays are generated by bremsstrahlung in the hot core, the spectrum is expected to be exponential with the slope related to the electron temperature near peak compression. If the fuel shell is sufficiently dense, x-ray absorption (free-free scattering) occurs and the spectrum deviates from the expected exponential behavior, and this deviation can be used to infer the density of the compressed fuel.[41] The x-ray spectrum in Fig. 108.14 indicates significant absorption between 1 and 2 keV. The opacity of the fuel shell is proportional to $\rho^2 R T^{-1/4}$, where ρ is the mass density of the compressed fuel, ρR is its areal density, and T is the electron temperature (inferred from the slope of the spectrum). The 1-D radiation hydrodynamic code $LILAC$[42] has been used to estimate the mass density ρ and minimum temperature of the compressed fuel by adjusting the temperature of the cold fuel and the thermal conductivity of the
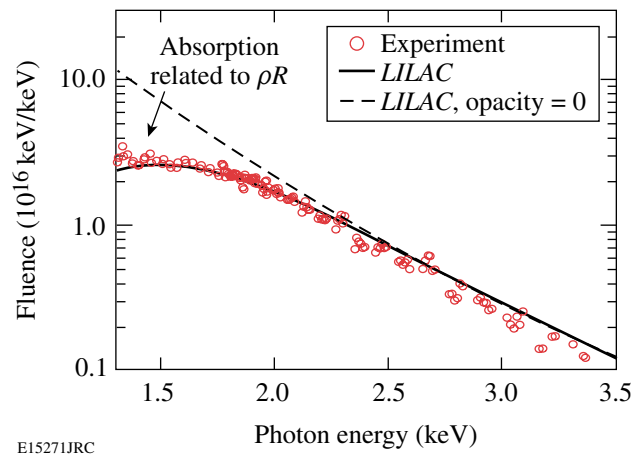

Figure 108.13
A measured secondary proton spectrum (solid circles) from a cryogenic D_2 implosion ($\alpha \sim 2$) is compared with the expected birth spectrum (shaded box). The protons lose energy as they pass through the dense fuel layer surrounding the hot core. The energy loss is proportional to the areal density of the dense fuel layer. For this implosion, the energy loss implies an areal density in excess of 100 mg/cm²; the low-energy tail suggests the peak areal density is well above 100 mg/cm².

Figure 108.14
Significant absorption is seen in the continuum x-ray spectrum emitted from the core of a cryogenic D_2 implosion ($\alpha \sim 1$) at x-ray energies below 2 keV. The emitted spectrum is expected to be exponential, and the deviation at low x-ray energies is consistent with a significant fuel areal density. The compressibility of the fuel shell in the 1-D radiation hydrocode $LILAC$ can be modified to fit the emitted spectrum to estimate the fuel density. The dashed line shows the expected exponential behavior of the x-ray emission if the opacity is artificially removed in the simulation.

hot core to match the emitted spectrum in both absolute fluence and shape (these adjustments mimic multidimensional mode growth and the consequent reduction in shell compression). The *LILAC* simulation that best agrees with the data is shown as the solid curve. The fuel density in the simulation suggests that ρR_{peak} may be as high as 190 ± 20 mg/cm^2. Two-dimensional simulations are underway to confirm this 1-D fuel-density estimate. The dashed curve in Fig. 108.14 is the predicted x-ray spectrum based on zero opacity. The curve is not purely exponential below 2 keV. If the opacity is calculated based on a purely exponential source spectrum and the density is taken from the *LILAC* simulation, the inferred ρR_{peak} would still be 180 mg/cm^2. Note that, if confirmed by further simulations, this estimate of the density represents a lower limit on the inferred peak areal density—if the density is less than predicted by the simulation, the measured opacity suggests that ρR_{peak} must be larger than the 180- to 190-mg/cm^2 estimate.

Summary

The cryogenic DT targets being imploded on OMEGA are energy-scaled versions of the baseline direct-drive-ignition design for the National Ignition Facility. This is the culmination of nearly three decades of research and development. Most of the components for the x-ray-drive ignition targets are at or near specification.

The β-layering process for producing a smooth inner ice surface in the direct-drive cryogenic DT targets imploded on OMEGA is well understood. The most important aspect of this process is controlling the symmetry of the isotherm on the outer surface of the capsule. This can now be done routinely, and over half of the cryogenic DT capsules imploded on OMEGA met the ignition requirement for the smoothness of the inner ice surface ($<$1-μm rms in all modes) at shot time. Optical shadowgraphy and phase-contrast imaging are used to characterize the inner ice surface for transparent (e.g., CH or CD shell) and opaque (e.g., Be and foam shells) ablators, respectively. The resolution of these techniques is adequate to characterize the ice smoothness to well below the ignition requirements for both direct and x-ray drives.

The Cryogenic Target Handling System on the OMEGA laser has deep roots in past work. Many of the fundamental concepts employed today were developed nearly three decades ago to perform the first cryogenic DT implosions using DT-filled, thin-glass-shell targets and two-beam irradiation. While these early target designs ultimately did not scale to ignition, the success of the current OMEGA program and the anticipated success of the future NIF ignition experiments owe much to these early pioneers.

REFERENCES

1. J. Nuckolls *et al.*, Nature **239**, 139 (1972).

2. W. J. Hogan, E. I. Moses, B. E. Warner, M. S. Sorem, and J. M. Soures, Nucl. Fusion **41**, 567 (2001).

3. P. W. McKenty, V. N. Goncharov, R. P. J. Town, S. Skupsky, R. Betti, and R. L. McCrory, Phys. Plasmas **8**, 2315 (2001).

4. J. D. Lindl, *Inertial Confinement Fusion: The Quest for Ignition and Energy Gain Using Indirect Drive* (Springer-Verlag, New York, 1998); J. D. Lindl *et al.*, Phys. Plasmas **11**, 339 (2004).

5. S. W. Haan *et al.*, Fusion Sci. Technol. **49**, 553 (2006); S. W. Haan *et al.*, Phys. Plasmas **12**, 056316 (2005); S. W. Haan *et al.*, Nucl. Fusion **44**, S171 (2004).

6. S. Atzeni and J. Meyer-ter-Vehn, *The Physics of Inertial Fusion: Beam Plasma Interaction, Hydrodynamics, Hot Dense Matter*, International Series of Monographs on Physics (Clarendon Press, Oxford, 2004).

7. T. R. Boehly, D. L. Brown, R. S. Craxton, R. L. Keck, J. P. Knauer, J. H. Kelly, T. J. Kessler, S. A. Kumpan, S. J. Loucks, S. A. Letzring, F. J. Marshall, R. L. McCrory, S. F. B. Morse, W. Seka, J. M. Soures, and C. P. Verdon, Opt. Commun. **133**, 495 (1997).

8. C. Stoeckl, C. Chiritescu, J. A. Delettrez, R. Epstein, V. Yu. Glebov, D. R. Harding, R. L. Keck, S. J. Loucks, L. D. Lund, R. L. McCrory, P. W. McKenty, F. J. Marshall, D. D. Meyerhofer, S. F. B. Morse, S. P. Regan, P. B. Radha, S. Roberts, T. C. Sangster, W. Seka, S. Skupsky, V. A. Smalyuk, C. Sorce, J. M. Soures, R. P. J. Town, J. A. Frenje, C. K. Li, R. D. Petrasso, F. H. Séguin, K. Fletcher, S. Padalino, C. Freeman, N. Izumi, R. Lerche, and T. W. Phillips, Phys. Plasmas **9**, 2195 (2002).

9. T. C. Sangster, J. A. Delettrez, R. Epstein, V. Yu. Glebov, V. N. Goncharov, D. R. Harding, J. P. Knauer, R. L. Keck, J. D. Kilkenny, S. J. Loucks, L. D. Lund, R. L. McCrory, P. W. McKenty, F. J. Marshall, D. D. Meyerhofer, S. F. B. Morse, S. P. Regan, P. B. Radha, S. Roberts, W. Seka, S. Skupsky, V. A. Smalyuk, C. Sorce, J. M. Soures, C. Stoeckl, K. Thorp, J. A. Frenje, C. K. Li, R. D. Petrasso, F. H. Séguin, K. A. Fletcher, S. Padalino, C. Freeman, N. Izumi, J. A. Koch, R. A. Lerche, M. J. Moran, T. W. Phillips, and G. J. Schmid, Phys. Plasmas **10**, 1937 (2003).

10. P. W. McKenty, T. C. Sangster, M. Alexander, R. Betti, R. S. Craxton, J. A. Delettrez, L. Elasky, R. Epstein, A. Frank, V. Yu. Glebov, V. N. Goncharov, D. R. Harding, S. Jin, J. P. Knauer, R. L. Keck, S. J. Loucks, L. D. Lund, R. L. McCrory, F. J. Marshall, D. D. Meyerhofer, S. P. Regan, P. B. Radha, S. Roberts, W. Seka, S. Skupsky, V. A. Smalyuk, J. M. Soures, K. A. Thorp, M. Wozniak, J. A. Frenje, C. K. Li, R. D. Petrasso, F. H. Séguin, K. A. Fletcher, S. Padalino, C. Freeman, N. Izumi, J. A. Koch, R. A. Lerche, M. J. Moran, T. W. Phillips, G. J. Schmid, and C. Sorce, Phys. Plasmas **11**, 2790 (2004).

11. F. J. Marshall, R. S. Craxton, J. A. Delettrez, D. H. Edgell, L. M. Elasky, R. Epstein, V. Yu. Glebov, V. N. Goncharov, D. R. Harding, R. Janezic, R. L. Keck, J. D. Kilkenny, J. P. Knauer, S. J. Loucks, L. D. Lund, R. L. McCrory, P. W. McKenty, D. D. Meyerhofer, P. B. Radha, S. P. Regan, T. C. Sangster, W. Seka, V. A. Smalyuk, J. M. Soures, C. Stoeckl, S. Skupsky, J. A. Frenje, C. K. Li, R. D. Petrasso, and F. H. Séguin, Phys. Plasmas **12**, 056302 (2005).

12. J. D. Sethian *et al.*, Nucl. Fusion **43**, 1693 (2003); J. D. Lindl, B. A. Hammel, B. G. Logan, D. D. Meyerhofer, S. A. Payne, and J. D. Sethian, Plasma Phys. Control. Fusion **45**, A217 (2003); R. L. McCrory, S. P. Regan, S. J. Loucks, D. D. Meyerhofer, S. Skupsky, R. Betti, T. R. Boehly, R. S. Craxton, T. J. B. Collins, J. A. Delettrez, D. Edgell, R. Epstein, K. A. Fletcher, C. Freeman, J. A. Frenje, V. Yu. Glebov, V. N. Goncharov, D. R. Harding, I. V. Igumenshchev, R. L. Keck, J. D. Kilkenny, J. P. Knauer, C. K. Li, J. Marciante, J. A. Marozas, F. J. Marshall, A. V. Maximov, P. W. McKenty, J. Myatt, S. Padalino, R. D. Petrasso, P. B. Radha, T. C. Sangster, F. H. Séguin, W. Seka, V. A. Smalyuk, J. M. Soures, C. Stoeckl, B. Yaakobi, and J. D. Zuegel, Nucl. Fusion **45**, S283 (2005).

13. V. A. Smalyuk, V. N. Goncharov, J. A. Delettrez, F. J. Marshall, D. D. Meyerhofer, S. P. Regan, and B. Yaakobi, Phys. Rev. Lett. **87**, 155002 (2001).

14. R. Betti, V. Lobatchev, and R. L. McCrory, Phys. Rev. Lett. **81**, 5560 (1998).

15. S. P. Regan, J. A. Marozas, R. S. Craxton, J. H. Kelly, W. R. Donaldson, P. A. Jaanimagi, D. Jacobs-Perkins, R. L. Keck, T. J. Kessler, D. D. Meyerhofer, T. C. Sangster, W. Seka, V. A. Smalyuk, S. Skupsky, and J. D. Zuegel, J. Opt. Soc. Am. B **22**, 998 (2005).

16. S. H. Glenzer *et al.*, Phys. Plasmas **7**, 2585 (2000).

17. T. M. Henderson and R. R. Johnson, Appl. Phys. Lett. **31**, 18 (1977).

18. J. R. Miller, in *Advances in Cryogenic Engineering*, edited by K. D. Timmerhaus (Plenum Press, New York, 1978), Vol. 23, pp. 669–675.

19. D. L. Musinski *et al.*, Appl. Phys. Lett. **34**, 300 (1979).

20. F. J. Marshall, S. A. Letzring, C. P. Verdon, S. Skupsky, R. L. Keck, J. P. Knauer, R. L. Kremens, D. K. Bradley, T. Kessler, J. Delettrez, H. Kim, J. M. Soures, and R. L. McCrory, Phys. Rev. A **40**, 2547 (1989).

21. R. L. McCrory, J. M. Soures, C. P. Verdon, F. J. Marshall, S. A. Letzring, S. Skupsky, T. J. Kessler, R. L. Kremens, J. P. Knauer, H. Kim, J. Delettrez, R. L. Keck, and D. K. Bradley, Nature **335**, 225 (1988).

22. J. K. Hoffer and L. R. Foreman, Phys. Rev. Lett. **60**, 1310 (1988).

23. A. J. Martin, R. J. Simms, and D. L. Musinski, *KMS Annual Technical Report*, 99, KMS Fusion, Inc., Ann Arbor, MI, KMSF Report No. 1348 (1985) (unpublished).

24. A. J. Martin, R. J. Simms, and R. B. Jacobs, J. Vac. Sci. Technol. A **6**, 1885 (1988).

25. G. W. Collins *et al.*, J. Vac. Sci. Technol. A **14**, 2897 (1996).

26. D. R. Harding, D. D. Meyerhofer, S. J. Loucks, L. D. Lund, R. Janezic, L. M. Elasky, T. H. Hinterman, D. H. Edgell, W. Seka, M. D. Wittman, R. Q. Gram, D. Jacobs-Perkins, R. Early, T. Duffy, and M. J. Bonino, Phys. Plasmas **13**, 056316 (2006).

27. M. J. Bonino, "Material Properties of Spider Silk," M.S. Thesis, University of Rochester, 2003.

28. J. D. Moody *et al.*, J. Phys. IV France **133**, 863 (2006).

29. J. Edwards *et al.*, Phys. Plasmas **12**, 056318 (2005).

30. J. A. Koch *et al.*, Fusion Technol. **38**, 123 (2000).

31. D. H. Edgell, W. Seka, R. S. Craxton, L. M. Elasky, D. R. Harding, R. L. Keck, and M. D. Wittman, Fusion Sci. Technol. **49**, 616 (2006).

32. D. S. Montgomery, A. Nobile, and P. J. Walsh, Rev. Sci. Instrum. **75**, 3986 (2004); B. J. Kozioziemski *et al.*, J. Appl. Phys. **97**, 063103 (2005).

33. S. Pollaine and S. Hatchett, Nucl. Fusion **44**, 117 (2004).

34. D. H. Edgell, W. Seka, R. S. Craxton, L. M. Elasky, D. R. Harding, R. L. Keck, L. D. Lund, and M. D. Wittman, J. Phys. IV France **133**, 903 (2006); D. S. Montgomery *et al.*, J. Phys. IV France **133**, 869 (2006).

35. *LLE Review Quarterly Report* **23**, 125, Laboratory for Laser Energetics, University of Rochester, Rochester, NY, LLE Document No. DOE/SP40200-03 (1985).

36. T. P. Bernat *et al.*, Phys. IV France **133**, 857 (2006).

37. P. B. Radha, J. Delettrez, R. Epstein, V. Yu. Glebov, R. Keck, R. L. McCrory, P. McKenty, D. D. Meyerhofer, F. Marshall, S. P. Regan, S. Roberts, T. C. Sangster, W. Seka, S. Skupsky, V. Smalyuk, C. Sorce, C. Stoeckl, J. Soures, R. P. J. Town, B. Yaakobi, J. Frenje, C. K. Li, R. Petrasso, F. Séguin, K. Fletcher, S. Padalino, C. Freeman, N. Izumi, R. Lerche, and T. W. Phillips, Phys. Plasmas **9**, 2208 (2002).

38. F. H. Séguin, J. A. Frenje, C. K. Li, D. G. Hicks, S. Kurebayashi, J. R. Rygg, B.-E. Schwartz, R. D. Petrasso, S. Roberts, J. M. Soures, D. D. Meyerhofer, T. C. Sangster, J. P. Knauer, C. Sorce, V. Yu. Glebov, C. Stoeckl, T. W. Phillips, R. J. Leeper, K. Fletcher, and S. Padalino, Rev. Sci. Instrum. **74**, 975 (2003).

39. B. Yaakobi, R. Epstein, and F. J. Marshall, Phys. Rev. A **44**, 8429 (1991).

40. V. A. Smalyuk, P. B. Radha, J. A. Delettrez, V. Yu. Glebov, V. N. Goncharov, D. D. Meyerhofer, S. P. Regan, S. Roberts, T. C. Sangster, J. M. Soures, C. Stoeckl, J. A. Frenje, C. K. Li, R. D. Petrasso, and F. H. Séguin, Phys. Rev. Lett. **90**, 135002 (2003); J. A. Frenje, C. K. Li, F. H. Séguin, J. Deciantis, S. Kurebayashi, J. R. Rygg, R. D. Petrasso, J. Delettrez, V. Yu. Glebov, C. Stoeckl, F. J. Marshall, D. D. Meyerhofer, T. C. Sangster, V. A. Smalyuk, and J. M. Soures, Phys. Plasmas **11**, 2798 (2003).

41. F. J. Marshall, J. A. Delettrez, R. Epstein, and B. Yaakobi, Phys. Rev. E **49**, 4381 (1994).

42. M. C. Richardson, P. W. McKenty, F. J. Marshall, C. P. Verdon, J. M. Soures, R. L. McCrory, O. Barnouin, R. S. Craxton, J. Delettrez, R. L. Hutchison, P. A. Jaanimagi, R. Keck, T. Kessler, H. Kim, S. A. Letzring, D. M. Roback, W. Seka, S. Skupsky, B. Yaakobi, S. M. Lane, and S. Prussin, in *Laser Interaction and Related Plasma Phenomena*, edited by H. Hora and G. H. Miley (Plenum Publishing, New York, 1986), Vol. 7, pp. 421–448.